

Technical Paper

Measuring desiccation-induced tensile stress during cracking process [☆]

Mai Sawada ^{*}, Yusuke Sumi, Mamoru Mimura

Department of Urban Management, Graduate School of Engineering, Kyoto University, Japan

Received 24 June 2020; received in revised form 3 January 2021; accepted 7 March 2021

Available online 27 May 2021

Abstract

The desiccation cracking of soil occurs when shrinkage is restricted during the drying process and the induced tensile stress equals the tensile strength. Thus far, experimental estimations of the tensile stress of soil have not been realized, although such estimates are important for predicting crack initiation. This study presents the development of a laboratory-based desiccation stress test to measure the tensile stress generated during the drying process until crack initiation. In this proposed desiccation stress test, the tensile stress is induced during the drying process in the longitudinal direction of bar-shaped specimens with fixed ends. Desiccation stress tests were performed on sandy soil with a rich fine fraction, and the results were verified through photographic observations of crack initiation and comparisons with the results of direct tension tests. The results show that the desiccation stress test yields reliable tensile stress until cracking. The application of the desiccation test results is illustrated via the verification of an existing model of crack initiation by desiccation. The results of the desiccation stress tests are useful for determining the model parameters that significantly influence the development of tensile stress and enable its accurate prediction until crack initiation.

© 2021 Production and hosting by Elsevier B.V. on behalf of The Japanese Geotechnical Society. This is an open access article under the CC BY-NC-ND license (<http://creativecommons.org/licenses/by-nc-nd/4.0/>).

Keywords: Desiccation cracking; Tensile stress; Tension test; Laboratory test; Cultural heritage

1. Introduction

Desiccation cracking occurs when the shrinkage of drying soil is restricted and the induced tensile stress becomes equal to the tensile strength. The cracking mechanism during the drying process is different from that of slaking, caused by repetitive shrinking and swelling, and from the pore air pressure evolution in drying–wetting cycles. Desiccation cracking is a problem that is relevant in a wide range of fields, including geotechnical engineering, environmental engineering, and agriculture, because it can damage earth structures, trigger landslides, and significantly influence water transport in the ground. In particular, many studies have focused on desiccation cracking in clay liners used for waste isolation or in fine-grained tailings, because water

infiltration is accelerated by cracking and can result in serious groundwater pollution.

Desiccation cracking is also an important problem in the restoration of cultural heritage sites, such as tumuli. Tumuli were constructed throughout Japan from the middle of the 3rd century to the end of the 7th century. More than 150 thousand tumuli still exist, although many have been damaged by natural processes. Tumuli are vulnerable to earthquakes and heavy rainfall because the density of the earth mounds is low. The earth mounds are made of manually compacted sandy soils with fine fraction contents of approximately 40%. The manual compaction energy is equivalent to 10–20% of the standard Proctor compaction energy (Mimura et al., 2015; Sawada et al., 2016). In many cases, the damaged tumuli are temporarily covered with plastic sheets before restoration work to prevent further damage due to precipitation. However, this promotes the desiccation of the earth mounds because water infiltration into these mounds is restricted. Furthermore, evaporation

Peer review under responsibility of The Japanese Geotechnical Society.

^{*} Corresponding author.

E-mail address: sawada.mai.6c@kyoto-u.ac.jp (M. Sawada).

from the earth mounds is allowed (Moriguchi et al., 2019). Water vapor flows out through the space between the plastic sheets and the earth mounds or condenses on the plastic sheets and flows downward due to gravity. Tumuli covered with plastic sheets dry in a short period of time. According to the report on the tumuli destroyed by the 2016 Kumamoto Earthquake (Agency for Cultural Affairs, 2017), the earth mounds dried in only a few months. The desiccation of the earth mounds lowered the plasticity of the mound soil, caused cracking, and made the restoration work more difficult. To prevent the deterioration of tumuli due to desiccation, it is necessary to understand the mechanical behavior of the drying earth mounds as an initial step. In particular, desiccation cracking that significantly influences the stability and hydro-thermal transport of the earth mounds should be studied.

Desiccation cracking results from the equilibrium between the induced tensile stress and the tensile strength. Hence, estimating the tensile stress is essential for fundamentally understanding and predicting desiccation cracking. Towner (1987) assumed that the tensile stress induced during the cracking process is equivalent in magnitude to the change in suction from the initial value. In this study, desiccation tests were conducted on dog bone-shaped clay bars and the gravimetric water content was measured at cracking. The tensile stress induced during the cracking process was estimated from a soil water characteristic curve based on this hypothesis. The estimated tensile stress was almost equal to the tensile strength at the water content when the cracks occurred, but was larger than the tensile strength at higher water contents before cracking. Towner (1987) concluded that the experimental results that were incompatible with the hypothesis could be attributed to anisotropic shrinkage caused by the restriction of shrinkage in the longitudinal direction. However, a quantitative estimation of the tensile stress could not be achieved. This shows that the tensile stress induced during the cracking process is highly influenced by the boundary conditions and cannot be easily estimated from the change in suction.

The tensile stress generated during the cracking process has been estimated in previous studies using numerical analyses. Rodríguez et al. (2007) performed a numerical analysis using a vertical 1-D model, restricted by lateral strain, to simulate the crack initiation of a drying circular clay sample. The crack initiation was predicted by comparing the experimentally obtained tensile strength with the calculated induced horizontal stress. Jommi et al. (2016) and Tollenaar (2017) performed similar calculations and studied the influence of the drying rate on the tensile stress profiles. The modeling of desiccation cracks has developed to the point of predicting 2-D and 3-D crack patterns by the implementation of numerical techniques to express the evolution of discontinuities (e.g., Trabelsi et al., 2012; Sánchez et al., 2014). However, an experimental estimation of the tensile stress that is induced until crack initiation has not been achieved. If it is possible to measure the tensile

stress through laboratory tests, these measurements will help with the understanding of its actual behavior. Furthermore, such measurements can be used to validate numerical simulations of desiccation cracking and will contribute to the development of numerical models that can predict crack initiation and propagation.

The aim of this study was to develop a laboratory test to measure the tensile stress induced in drying specimens until crack initiation (hereafter referred to as “desiccation stress test”). The desiccation stress test proposed in this study was used to measure the induced tensile stress of bar-shaped drying specimens with fixed ends. Desiccation stress tests were carried out on 13 specimens of sandy soil with a rich fine fraction obtained from a tumulus mound. Herein, the methodology of the desiccation stress test is firstly presented. The hydraulic properties and mechanical properties, in particular, the tensile strength of the specimens, are then described. The relationship between the tensile strength and the gravimetric water content is obtained through direct tension tests on drying specimens. Tensile strength is another important factor that influences cracking. Finally, the results of the desiccation stress tests are shown. The behavior of the tensile stress throughout the cracking process is examined, and the application of the desiccation stress test results is illustrated via the verification of an existing model of crack initiation by desiccation.

2. Experimental methods

2.1. Methodology

Fig. 1 shows a conceptual diagram of the desiccation stress test, which contained bar-shaped drying soil specimens with fixed ends. Tensile stress was induced in the longitudinal direction on the cross-section of each bar because the shrinkage of the bar was restricted. The tensile stress increased as the bar dried, and cracks occurred when the tensile stress reached the tensile strength. This induced tensile stress was measured with the proposed desiccation stress test. Fig. 2 presents the methodology of the desiccation stress test. Both ends of the restraint device were anchored to the specimen, while the middle portion was unanchored. The role of the restraint device was to prevent shrinkage in the longitudinal direction of the specimen during the drying process until crack initiation. The restraint device was assumed to be stiffer than the specimen, and both ends had rough surfaces. It is important to note that the restraint device did not prevent shrinkage in the lateral and vertical directions. Water was able to evaporate from each face of the specimen. Thus, in the unanchored section, tensile force was generated in the longitudinal direction on the cross-section of the specimen as the specimen dried, whereas compressive force equal in magnitude to the tensile force was generated in the restraint device. These forces formed an action-reaction force pair, which increased until tensile cracks occurred. The induced tensile force could not be measured directly, but could be obtained by calculating

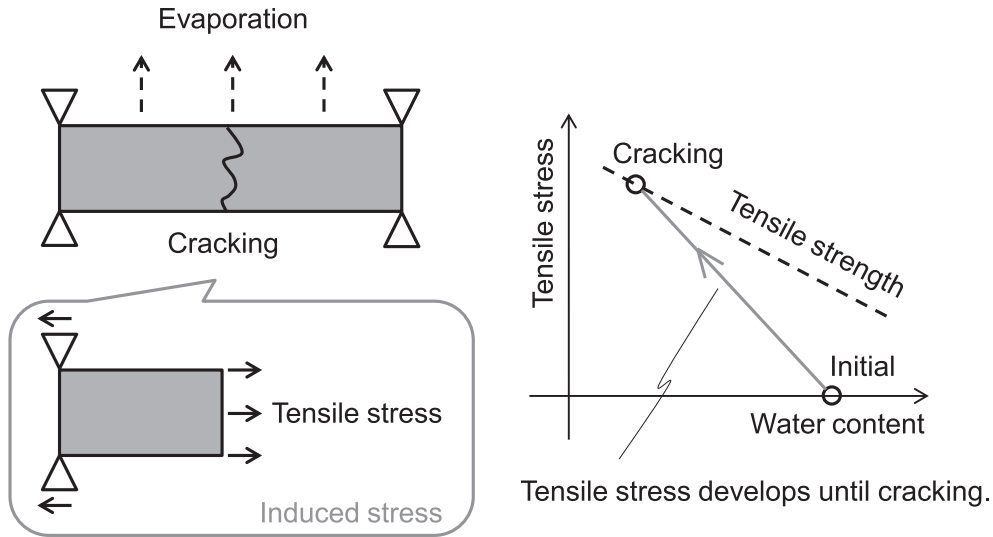


Fig. 1. Tensile stress induced in drying bar-shaped specimen with fixed ends.

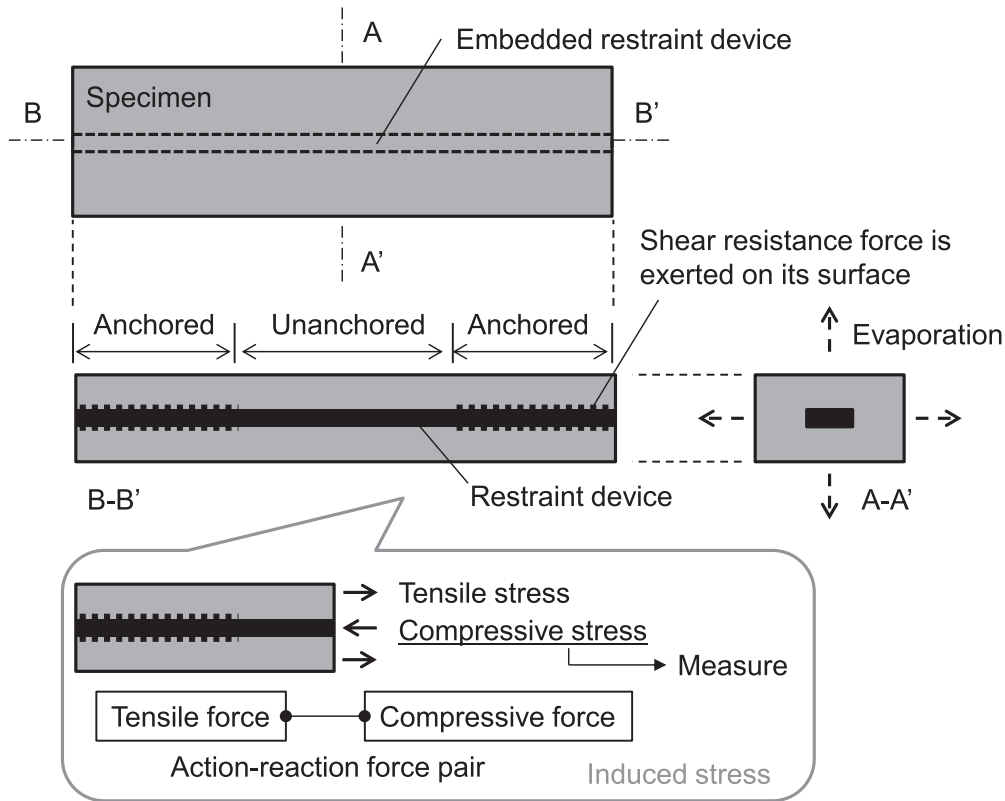


Fig. 2. Methodology of desiccation stress test.

the compressive force using the compressive strain of the restraint device measured by strain gauges. Thus, the induced tensile stress was obtained by dividing the tensile force by the cross-sectional area of the specimen.

The desiccation stress test was inspired by the autogenous shrinkage stress test for concrete proposed by Matsushita and Tsuruta (1999) and Ohno and Nakagawa (1999). The autogenous shrinkage of concrete is due to the consumption of water in the hydration process. In the

autogenous shrinkage stress test, the induced tensile force of a reinforced concrete bar (100 mm × 100 mm × 1500 mm) is measured by strain gauges attached to the reinforcing bar. The specimen and equipment used for the desiccation stress test were designed by considering the differences in dewatering mechanisms and the magnitudes of the tensile forces induced by the restriction of shrinkage between the desiccation shrinkage of the soil and the autogenous shrinkage of the concrete.

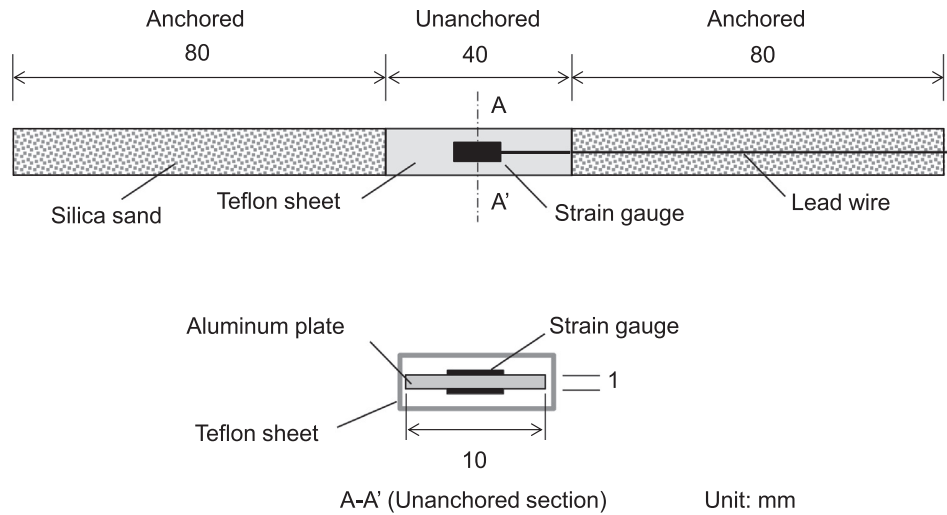


Fig. 4. Restraint device.

measurements was $0.6 \text{ kN/m}^2 \cdot \mu\text{s}$. If the stiffness (i.e., Young’s modulus \times cross-sectional area) of a restraint device is very large, only a little compressive strain will be measured. This means that the measured tensile stress corresponding to $1 \mu\text{s}$ is large; and thus, the resolution is lower.

The length of the anchored sections is an important factor in accurately measuring the tensile stress, because the restraint device is anchored to the specimen with shear resistance force exerted on its interfaces. If the anchoring length is insufficient, the compressive force of the restraint device will exceed the capacity of the shear resistance force in the anchored sections, and the restraint device will tear loose from the specimen. The anchoring length of the restraint device used in this study was 80 mm. In the anchored sections, air-dried silica sand was attached to the aluminum plate with double-sided adhesive tape to enhance the capacity of the shear resistance force of the anchored sections. The grain size distribution curve of the silica sand is shown in Fig. 5.

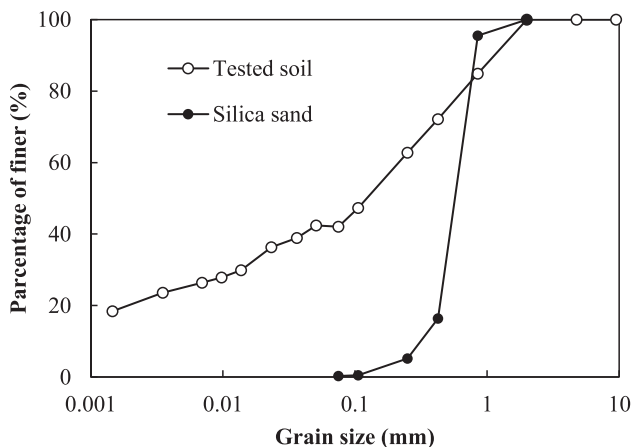


Fig. 5. Grain size distribution curves.

The length of the unanchored section was 40 mm. After attaching the strain gauges, the middle section of the restraint device was wrapped with a greased Teflon sheet, $40 \text{ mm} \times 25 \text{ mm}$, to eliminate any adhesion between the restraint device and the specimen.

2.4. Temperature and humidity

Desiccation stress tests were performed in a constant climate chamber (ESPEC Co., Ltd., LHL-114) in which the temperature and relative humidity were kept constant at $20 \text{ }^\circ\text{C}$ ($\pm 0.3 \text{ }^\circ\text{C}$) and $60\% \text{ RH}$ ($\pm 0.7\% \text{ RH}$), respectively. This hydrothermal environment corresponds to a suction of 70 MPa . Pore water evaporated from the surfaces of the specimen until the suction of the soil and the atmosphere had reached equilibrium in the same manner as that of the vapor-pressure method used in the water retention test.

A specimen with Teflon sheets used for the specimen preparation was mounted on an electric balance and placed in the constant climate chamber. The Teflon sheets were removed from the side faces to allow water to evaporate through them. The gravimetric water content of each specimen during the test was calculated using the mass of evaporation. The volume of the specimen was not directly measured, but the degree of saturation was estimated using the shrinkage curve (void ratio vs. gravimetric water content) described in Section 3.1. In laboratory tests, the measurement of the mass of a specimen is generally more reliable than that of its volume. This is particularly true for laboratory tests accompanied by crack generation, because the volume is calculated from the external dimensions of the specimen, although inner cracks can occur. For this reason, in previous experimental studies on desiccation cracking, the degree of saturation of drying specimens with cracks was not monitored, and the test results were analyzed only in terms of their gravimetric water contents

(e.g., Towner, 1987; Péron et al., 2005; Nahlawi and Kodikara, 2006).

3. Tested soil

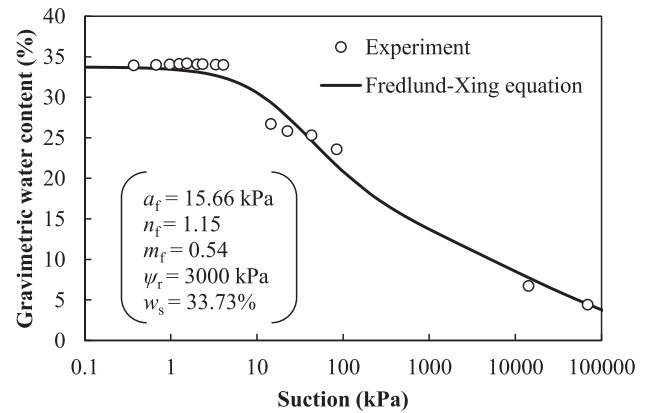
3.1. Material properties

Mound soil from the Kengoshizuka Tumulus at Asuka Village in Nara Prefecture, Japan was used, after it had passed through a 2-mm sieve. The residual soil originated from granites and granodiorites, and is widely distributed in the village. According to the results of X-ray diffraction analyses performed on mound soil from another tumulus in the village, the soil consists of quartz, chlorite, smectite, plagioclase, and muscovite (Agency for Cultural Affairs et al., 2017). Table 1 lists the basic properties, while Fig. 5 shows the grain size distribution curve of the tested soil. Desiccation stress tests were performed on the specimens with an initial gravimetric water content of 29% and an initial dry density of 1.37 g/cm³. The initial water content corresponded to the natural water content of the tumulus mound, and the initial dry density was approximately equal to the *in situ* dry density of the tumulus mound (Sawada et al., 2016).

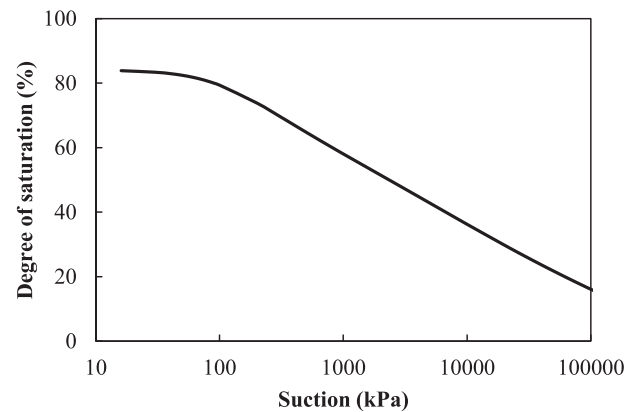
Fig. 6 (a) shows the experimentally obtained drying branch of the soil water characteristic curve as a function of the gravimetric water content (w-SWCC). The experimental results were obtained using one of the three methods according to the range in suction, namely, the water-column method (0–5 kPa), the pressure-plate method (5–100 kPa), or the vapor-pressure method (above 14 MPa). Herein, the suction employed in the water-column and pressure-plate methods was matric suction, whereas the suction employed in the vapor-pressure method was total suction. Soil suction is generally defined in terms of matric suction from 0 to 1500 kPa, while soil suction is defined in terms of total suction from 1500 kPa to 1000 MPa (e.g., Fredlund and Xing, 1994). In the water-column and pressure-plate methods, a specimen, 50 mm in diameter and 50 mm in height and compacted at a dry density of 1.37 g/cm³, was used. The initial gravimetric water content was 29%. The specimen was mounted on a ceramic disk with an air-entry value of 100 kPa in a pressure cell and saturated by connecting the bottom of the specimen to a water column. During saturation, the water level of the column was kept at the same level as the top of the specimen. The suction of the specimen and the water column reached

Table 1
Properties of tested soil.

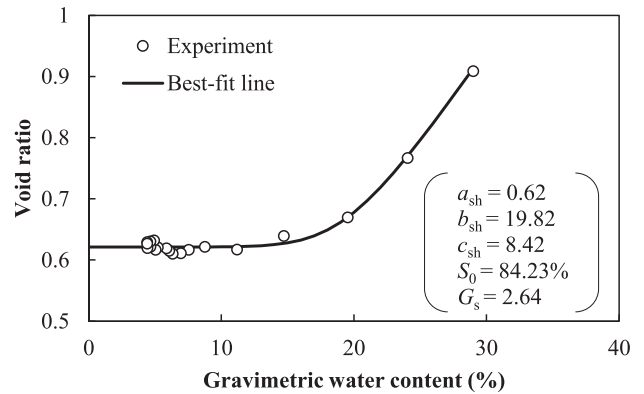
Specific gravity	2.64
Gravimetric water content (%)	29.0
Maximum dry density (g/cm ³)	1.70
Optimum water content (%)	18.0
Shrinkage limit (%)	25.2
Plastic limit (%)	23.1
Liquid limit (%)	37.5



(a) w-SWCC



(b) s-SWCC



(c) Shrinkage curve

Fig. 6. Drying branches of soil water characteristic curves and shrinkage curve.

equilibrium in a week, and the specimen was fully saturated. The water column was decreased by 50 cm in several steps, and air pressures of 10 kPa, 20 kPa, 40 kPa, and 80 kPa were then applied to the top of the specimen. During each step, the amount of water that drained from the specimen was measured and the gravimetric water content at the equilibrium state was estimated. In the vapor-pressure method, two specimens were used. The specimens were prepared in the same manner as for the desiccation

stress test presented in Section 2.2, but without the installation of the restraint device. One specimen was placed at constant climatic conditions of a temperature of 20 °C and relative humidity of 60% RH (suction of 70 MPa), while the other specimen was placed at conditions of 20 °C and 90% RH (suction of 14 MPa) until the masses of the specimens became constant. Then, the gravimetric water contents at the equilibrium state were estimated from the masses of evaporated water.

The laboratory-obtained w-SWCC was fitted to the Fredlund-Xing equation (Fredlund and Xing, 1994), modified by Fredlund (2017), to yield the following relationship between gravimetric water content w and suction ψ :

$$w(\psi) = \frac{w_s(1 - \ln(1 + \psi/\psi_r)/\ln(1 + 10^6/\psi_r))}{(\ln(\exp(1) + (\psi/a_f)^{n_f}))^{m_f}} \quad (2)$$

where w_s and ψ_r are the initial gravimetric water content and the suction close to the residual conditions, respectively. Parameters a_f , n_f , and m_f are fitting parameters. This equation has the advantage of fitting the experimental data over the entire suction range from 0 to 1000 MPa (Fredlund and Xing, 1994). The best-fit parameters estimated using the least-squares method are shown in Fig. 6 (a). The suction near residual condition ψ_r was determined within the recommended values of Fredlund and Xing (1994) (i.e., 1500–3000 kPa). Following the procedures proposed by Fredlund (2017), the w-SWCC was converted to the degree of saturation vs. suction (s-SWCC), given in Fig. 6 (b), using the shrinkage curve shown in Fig. 6 (c). The shrinkage curve was obtained by measuring the volume of the specimen during the water retention test using the vapor-pressure method at a temperature of 20 °C and relative humidity of 60% RH. The volume of the specimen was obtained by taking a photo every 3 h using a camera set above the specimen, and reading the length and width from the photos using AutoCAD (AUTODESK). The strain of the height was assumed to be the average of those of the length and width. The differences between the estimated and measured dimensions after testing were less than 1 mm. The experimentally obtained shrinkage curve was fitted to the following equation proposed by Fredlund et al. (2002):

$$e(w) = a_{sh} \left(\left(\frac{w}{b_{sh}} \right)^{c_{sh}} + 1 \right)^{1/c_{sh}} \quad (3)$$

$$b_{sh} = a_{sh} \times S_0/G_s$$

where e is the void ratio, S_0 is the initial degree of saturation, and G_s is the specific gravity. Parameters a_{sh} , b_{sh} , and c_{sh} are fitting parameters. The best-fit parameters are shown in Fig. 6 (c).

3.2. Measurement capacity of tensile stress

In the desiccation stress test, the measurement capacity of the tensile stress is limited by the capacity of the shear resistance force exerted on the faces of the restraint device

in the anchored sections. The capacity of the shear resistance force in the anchored sections was investigated using the shear box test on a specimen simulating the interface between the restraint device and a specimen from the desiccation stress test. A shear box designed for a specimen, 60 mm in diameter and 20 mm in height, was used. The tested soil had a gravimetric water content of 29% and was compacted at a dry density of 1.37 g/cm³ in the lower half of the shear box. In the upper half of the shear box, an aluminum plate fixed on a resin base, 10 mm in height, was installed. The air-dried silica sand was attached to the surface of the aluminum plate in the same manner as the restraint device.

The test results are shown in Fig. 7. Angle of shear resistance ϕ was 16° and cohesion c was 25 kPa. Cohesion was exerted because the silica sand particles dug into the lower compacted soil. In the desiccation stress tests, only cohesion contributed to the shear resistance force in the anchored sections because no confining pressure was applied. The measuring capacity of the tensile stress, σ_{tmax} , can be estimated as follows:

$$\sigma_{tmax} = c \times A_a/A_s \quad (4)$$

where the total surface area of both faces of the restraint device in an anchored section, A_a , is 1600 (=10 × 80 × 2) mm². The cross-sectional area of the specimen, A_s , is 990 (=50 × 20–10 × 1) mm². Thus, the measuring capacity of the tensile stress was estimated to be 40.0 kN/m².

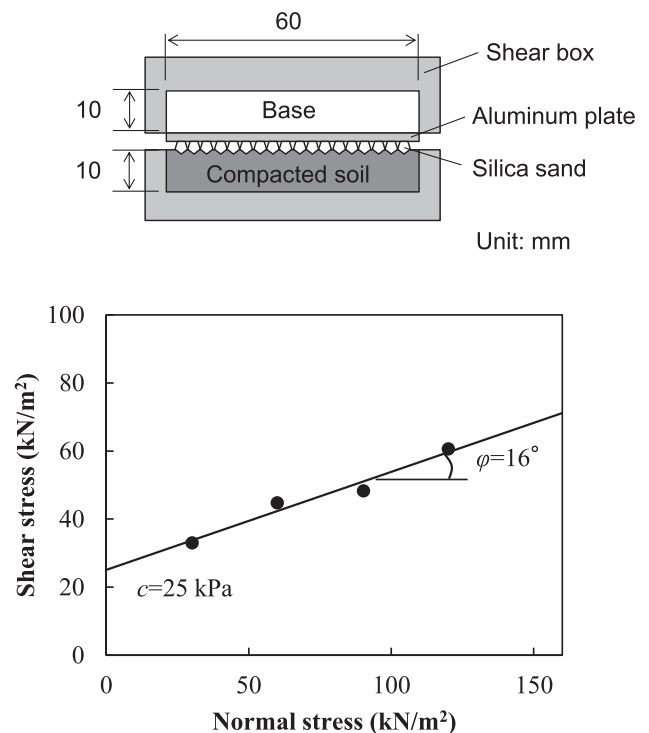


Fig. 7. Shear box test on interface between restraint device and specimen.

4. Tensile strength during desiccation process

4.1. Direct tension test

Tensile strength changes as the soil dries and is an important factor that influences cracking. Direct tension tests were performed on drying specimens to investigate the relationship between tensile stress and the gravimetric water content. Tensile strength can be obtained with three types of laboratory tests, namely, the direct tension test, the splitting tension test, and the bending test. Namikawa and Koseki (2007) conducted numerical simulations to investigate the applicability of these tests on cement-treated sand. They concluded that direct tension tests yield a reliable tensile strength when compared to the other two tests, which assume a linear elastic material to estimate tensile strength. Splitting tests underestimate the tensile stress due to the shear failure below the loading strip, whereas bending tests overestimate the tensile strength due to the redistribution of stresses with strain-softening.

In previous studies, direct tension tests have been performed on dog bone-shaped or hourglass-shaped specimens (e.g., Towner, 1987; Rodríguez et al., 2007; Trabelsi et al., 2012; Tollenaar, 2017) to investigate the tensile strength of drying soils. In the present study, direct tension tests were conducted on the same bar-shaped specimens as those used for the desiccation stress tests. The specimens were prepared using the same method as that presented in Section 2.2, but without the installation of the restraint device. Each specimen was mounted on an electric balance and placed under constant climatic conditions of a temperature of 20 °C and relative humidity of 60% for 2 h to 6 d to dry them to various gravimetric water contents. Each specimen was taken out of the constant climate chamber just before testing and its dimensions were measured with a caliper. Pieces of sandpaper (50 mm × 50 mm) were attached to both faces at the ends of each specimen with instant glue to set the specimen in the testing apparatus.

Fig. 8 shows the testing apparatus used for the direct tension tests. Each specimen was set in the apparatus by clipping the ends of the specimen. Although the clips have notches, the specimens slipped easily when they were pulled out without any sandpaper, which enhanced the friction between the clips and the specimens. The lower clip was fixed to the shaft, whereas the upper clip was connected to a revolving joint to avoid the flexural failure of the specimen. Each specimen was pulled out at a constant rate of 1 mm/min until it ruptured.

4.2. Relationship between tensile strength and gravimetric water content

The measured tensile strengths are plotted in Fig. 9. The tensile stress is seen to have increased significantly with the decrease in gravimetric water content. The relationship between the tensile strength and the gravimetric water content is approximated by Eq. (5). Trabelsi et al. (2012) also

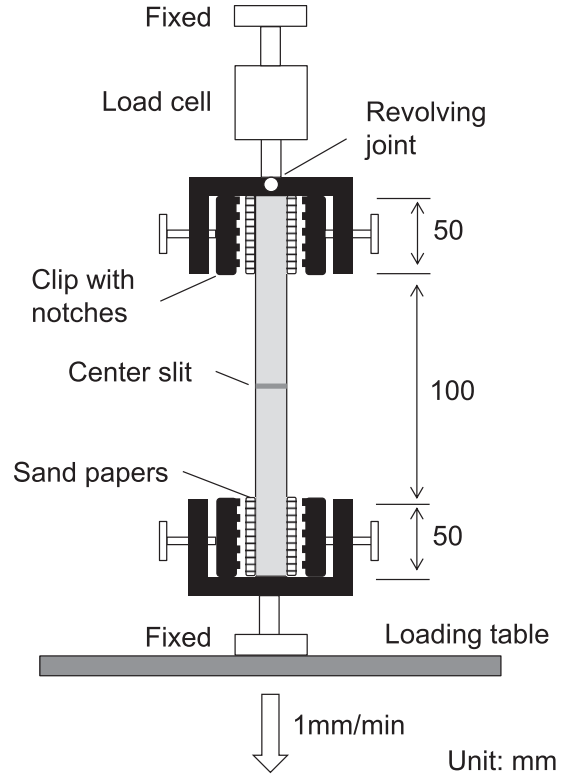


Fig. 8. Apparatus for direct tension test.

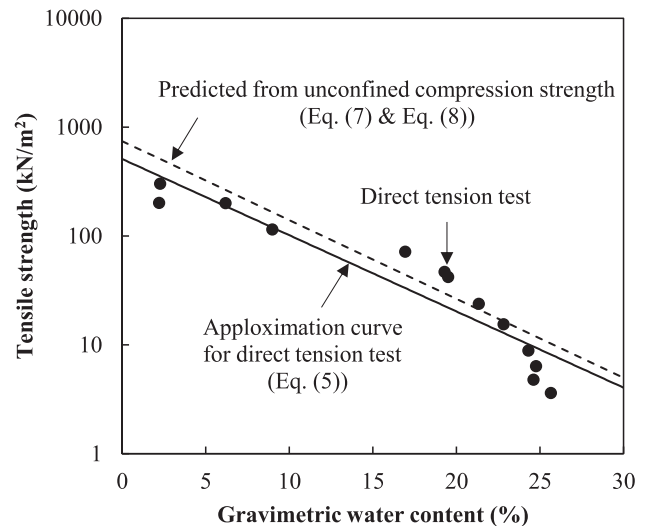


Fig. 9. Relationship between tensile strength and gravimetric water content.

represented the tensile strength–gravimetric water content relationship of a drying clayey soil using the following exponential equation:

$$\sigma_t = 509.14e^{-0.16w} \quad (R^2 = 0.88) \quad (5)$$

To validate the results of the tensile strength obtained with direct tension tests, the measurements were compared with the tensile strengths predicted from the unconfined compression strength. Trabelsi et al. (2012) proposed the

modified Mohr–Coulomb failure criterion shown in Fig. 10 that defines the relationship between the strength parameters and the tensile strength as

$$c = \frac{|\sigma_t|}{2} \left(\frac{1 + \sin\phi}{\cos\phi} \right) \quad (6)$$

where c is cohesion and ϕ is the internal friction angle. Thus, the relationship between the tensile strength and the unconfined compression strength, q_u , is expressed as follows:

$$|\sigma_t| = q_u \left(\frac{1 - \sin\phi}{1 + \sin\phi} \right) \quad (7)$$

Unconfined compression tests were performed on specimens 35 mm in diameter and 70 mm in height. The initial gravimetric water contents and dry densities were equivalent to those of the specimens used for the direct tension tests. Each specimen was prepared by compacting the test soil in a cylindrical mold and allowing it to dry in a constant climate chamber in the same manner as in the direct tension tests. The unconfined compression strength was plotted over a range of gravimetric water contents on a semi-log plot (Fig. 11) and is approximated as follows:

$$q_u = 1832.09e^{-0.17w} \quad (R^2 = 0.96) \quad (8)$$

The tensile strength–gravimetric water content relationship, predicted by substituting Eq. (8) for Eq. (7), is shown in Fig. 9. Internal friction angle ϕ was determined as 25° with shear box tests, and the dependence of ϕ on the water content was not considered. The tensile strength–gravimetric water content relationship, predicted from the unconfined compression strengths, overlies the results of the direct tension tests. Hence, assuming a modified Mohr–Coulomb failure criterion, the results of the direct tension tests are reliable.

5. Experimental results and discussion

5.1. Tensile stress behavior throughout cracking process

Desiccation stress tests were performed on 13 specimens. Fig. 12 shows a typical time history of the measured tensile stress, while Fig. 13 shows the time history of the change in gravimetric water contents of the specimens during the test. The tensile stress developed as the sample dried; it reached

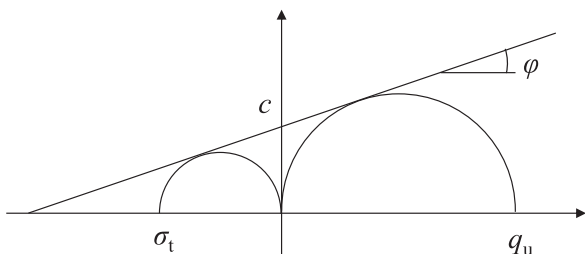


Fig. 10. Modified Mohr-Coulomb failure criterion.

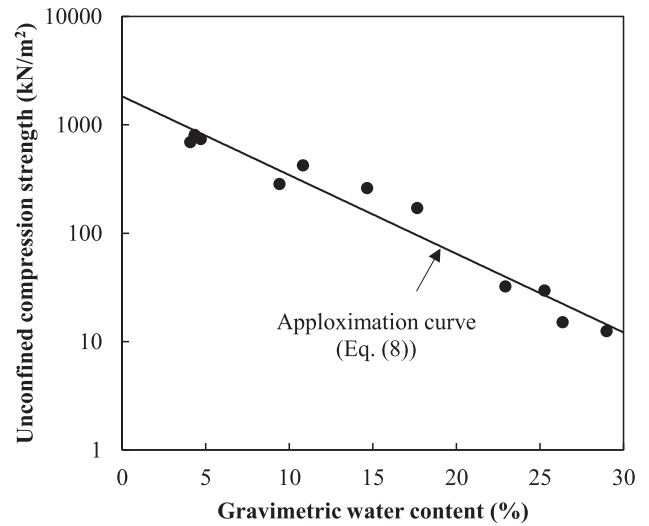


Fig. 11. Relationship between unconfined compression strength and gravimetric water content.

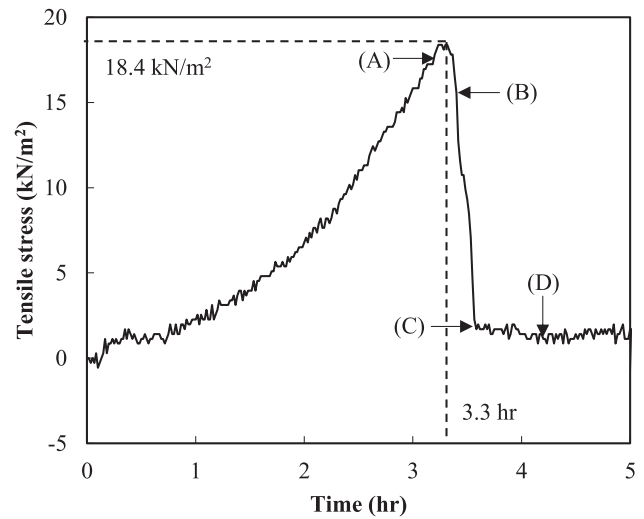


Fig. 12. Time history of tensile stress in cracking process.

its peak 3 h and 20 min after the start and then suddenly dropped. The gravimetric water content was 23.67% when the tensile stress was at its peak. Herein, changes in the cross-sectional area of the specimen were not considered, but the effect on the tensile stress at cracking was limited. The volumetric strain at cracking can be estimated as 8% from the shrinkage curve shown in Fig. 6 (c). Thus, the decrease in the cross-sectional area from the initial value will be approximately 8% when shrinkage in the longitudinal direction is restricted.

To understand the tensile stress behavior, photos of the specimens were taken every 10 min by a camera set above the specimen to observe the crack initiation. Fig. 14 shows photos of the middle portion of a specimen taken before and after cracking. Each photo was taken at the times indicated in Figs. 12 and 13. Up to 5 min before the tensile stress reached its peak (Fig. 14 (A)), no change was

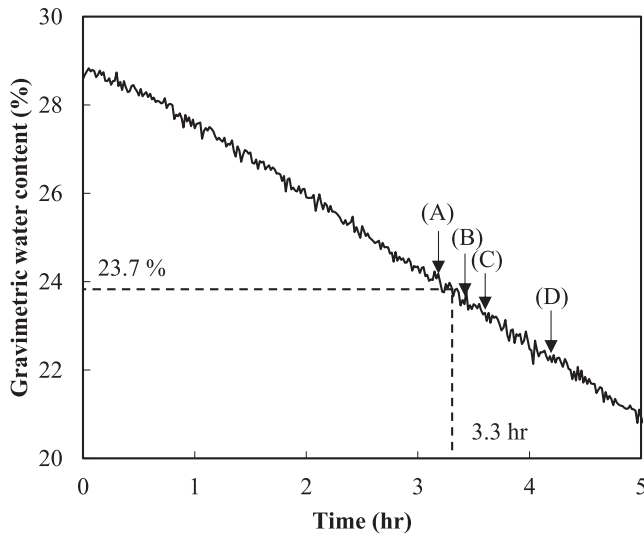


Fig. 13. Time history of gravimetric water content in cracking process.

observed. Five min after the tensile stress reached its peak, the center slit of the specimen opened slightly and a minor crack was observed (Fig. 14 (B)). The crack appeared clearly 10 min after the tensile stress had reached its peak (Fig. 14 (C)). At this time, the tensile stress dropped to almost zero. Fifty-five min after the tensile stress reached its peak, the width of the center slit had grown to 0.5 mm and the embedded restraint device appeared (Fig. 14 (D)). The photos show that the sudden drop in tensile stress was due to the opening of the crack. It is impossible to observe the crack initiation in the photos. Physically, however, it is reasonable to assume that the tensile stress reached its peak at the crack initiation, and that the peak value was equal to the tensile strength. After the crack initiation, the tensile force induced on the cross-section decreased because the cross-sectional area of the

specimen decreased as the crack opened. However, the tensile stress was estimated assuming that the cross-sectional area was constant; and hence, the estimated tensile stress apparently dropped.

These results show that the tensile stress behavior obtained with the desiccation stress tests is consistent with the cracking behavior. The estimation of the induced tensile stress through the cracking process is a significant advantage provided by the desiccation stress test, as it is useful for the validation of the numerical simulations of desiccation cracking and contributes to the development of numerical models that can predict crack initiation and propagation. Assuming that a crack initiates when the induced tensile stress is at its peak, the desiccation stress test also has the advantage of accurately detecting the crack initiation. In most previous studies, the crack initiation was observed visually using cameras. However, there is a time lag between the actual crack initiation and the observed crack initiation because visual observations cannot detect minor or inner cracks. During this time lag, the gravimetric water content will decrease and the tensile stress at cracking will therefore be overestimated if it is estimated from the tensile strength–gravimetric water content relationship.

5.2. Comparison with direct tension test results

Assuming that a crack initiates when the induced tensile stress is at its peak, the measurement values of the 13 specimens at cracking are listed in Table 2. Here, the degree of saturation at cracking was estimated using the shrinkage curve shown in Fig. 6 (c). The test results for Case 1 are discussed in Section 5.1. The peak tensile stress values (i.e., the tensile stress at cracking) are within the measurement capacity of 40.0 kN/m²; thus, the anchoring length of the restraint device is appropriate for the tests. The experimen-

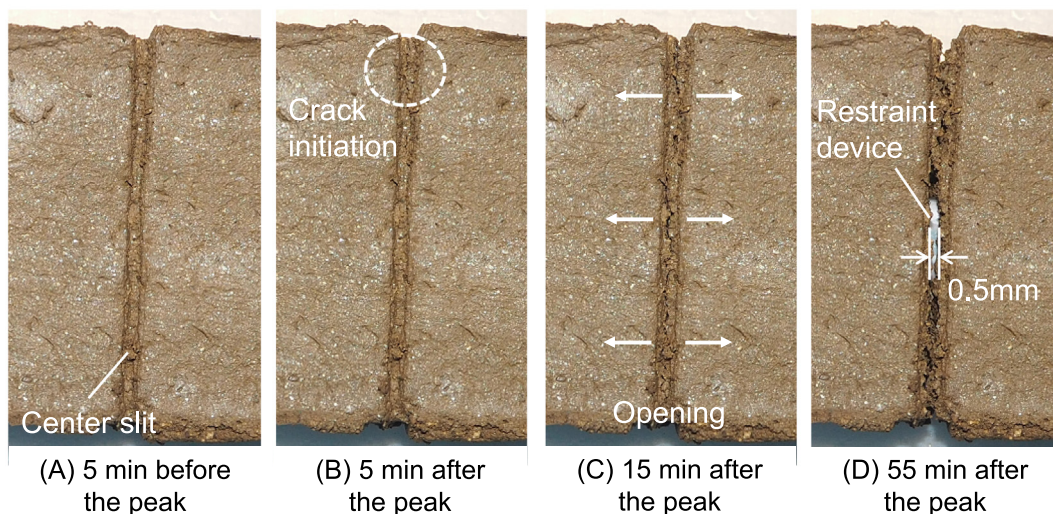


Fig. 14. Crack initiation and opening in middle of specimen.

Table 2
Measurement values at cracking.

Case	Time (hr)	Gravimetric water content (%)	Degree of saturation (%)	Tensile stress (kPa)
1	3.32	23.67	82.23	18.38
2	4.33	24.16	82.52	20.64
3	2.50	24.84	82.85	18.67
4	3.00	23.31	81.99	15.84
5	3.00	25.68	83.17	6.22
6	2.83	24.39	82.64	5.94
7	2.67	24.12	82.50	10.75
8	3.50	23.07	81.80	20.93
9	2.83	24.39	82.64	5.94
10	3.00	24.15	82.51	13.07
11	3.05	23.75	82.28	11.88
12	3.73	23.86	82.35	18.95
13	4.30	23.56	82.16	15.55
Max	4.33	25.68	83.17	20.93
Min	2.50	23.07	81.80	5.94
Mean value	3.24	24.07	82.43	14.06
Standard variation	0.56	0.65	0.35	5.33

tal conditions of the 13 cases are equivalent, but the results are varied because the tensile ruptures that initiated from the small defects were influenced significantly by the heterogeneity of the specimens. The results of the direct tension tests performed by Towner (1987) indicate that the tensile strength of drying clay specimens varies with their equivalent gravimetric water contents. The degrees of variation in tensile strength are equivalent to those of the peak values of the tensile stress measured with the desiccation stress tests.

To validate the results of the desiccation stress tests, the tensile stress at cracking was compared with the tensile strength obtained from the direct tension tests. Fig. 15 shows that the measurements of the tensile stress at cracking plot almost on the line for the tensile strength–gravimetric water content relationship shown in Fig. 9. This good agreement between the results of the desiccation

stress tests and those of the direct tension tests indicates that the former yielded quantitatively reliable tensile stress measurements until crack initiation. Fig. 15 can be drawn as a function of the degree of saturation, but the gravimetric water content is more expedient. This is because the gravimetric water content is raw measured data, whereas the degree of saturation is processed data that assumes that each specimen has the same shrinkage curve as that shown in Fig. 6 (c). The variations in the raw measured data decrease in this conversion process to those of the degree of saturation.

5.3. Contributions of desiccation stress tests to modeling desiccation cracking

As an example of the application of the results of the desiccation stress tests, an existing model for crack initiation by desiccation, proposed by Jommi et al. (2016), was verified by comparing the computed tensile stresses with the measured values. The tensile stresses induced during the desiccation stress tests were numerically predicted using the model and then compared with the measured values (Table 2).

The model assumed here is a simple incremental hypo-elastic model that describes the material stiffness as follows:

$$\begin{bmatrix} \dot{p}' \\ \dot{q} \end{bmatrix} = \begin{bmatrix} K & 0 \\ 0 & 3G \end{bmatrix} \begin{bmatrix} \dot{\epsilon}_{vol} \\ \dot{\epsilon}_d \end{bmatrix} \quad (9)$$

where K is the tangent bulk modulus and G is the shear modulus. The stress and strain variables are defined as follows:

$$\begin{aligned} p' &= \frac{1}{3}(2\sigma'_{LV} + \sigma'_{LO}) \\ q &= (\sigma'_{LV} - \sigma'_{LO}) \\ \epsilon_{vol} &= (2\epsilon_{LV} + \epsilon_{LO}) \\ \epsilon_d &= \frac{2}{3}(\epsilon_{LV} - \epsilon_{LO}) \end{aligned} \quad (10)$$

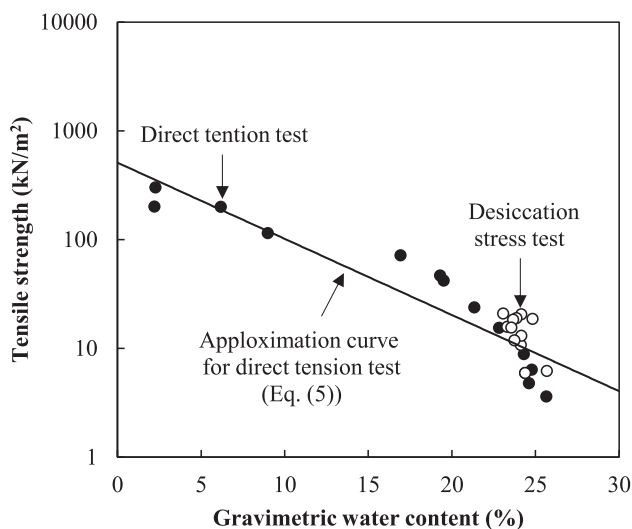


Fig. 15. Comparison with tensile strength measured with direct tension tests.

Herein, the stress and strain induced in the desiccation stress tests were assumed. The stress and strain in the lateral and vertical directions were assumed to be isotropic. Index *LV* represents the lateral and vertical directions, and *LO* represents the longitudinal direction. The volumetric strain rate, $\dot{\epsilon}_{vol}$, is defined as follows:

$$\dot{\epsilon}_{vol} = -\frac{\dot{e}_w}{1 + e_0} \tag{11}$$

where e_0 is the initial void ratio and water ratio e_w is defined as the ratio of the volume of water to the volume of solids. Eq. (11) is satisfied as long as the volumetric change is equal to the evaporation. Fig. 16 presents a comparison of the volumetric change and evaporation, created using the experimental data on the shrinkage curve given in Fig. 6 (c). It shows that the volumetric change was almost equivalent to evaporation until the gravimetric water content decreased to approximately 20%. As shown in Table 2, the gravimetric water content at cracking was greater than 20% (i.e., 23.07–25.68%). Thus, Eq. (11) is satisfied until crack initiation in the desiccation stress tests. The volumetric strain rate was assumed to increase proportionally to the increment in effective stress, \dot{p}' .

$$\dot{\epsilon}_{vol} = \frac{1}{K}\dot{p}' = \frac{1}{K}(\dot{p} + \dot{\psi}) \tag{12}$$

$$K = -(1 + e_0) \frac{\partial \psi}{\partial e_w} \tag{13}$$

where \dot{p} and $\dot{\psi}$ are the increments in mean stress and suction, respectively. In the desiccation stress tests, $\dot{\epsilon}_{vol}$ increased with an increase in $\dot{\psi}$ during the drying process because \dot{p} is zero. The water ratio and suction were assumed to change, maintaining the relationship of w-SWCC shown in Fig. 6 (a). Under the boundary condition of $\dot{\epsilon}_{LO} = 0$, the total stress increment in the longitudinal direction is given by

$$\dot{\sigma}_{LO} = \frac{2}{3}G \frac{\dot{e}_w}{1 + e_0} \tag{14}$$

$$G = \frac{3(1 - 2\nu)}{2(1 + \nu)}K \tag{15}$$

where ν is Poisson’s ratio. The Poisson’s ratio of the specimens for the desiccation stress tests was estimated from the results of triaxial tests under constant suction. Specimens, 50 mm in diameter and 100 mm in height, were prepared by compacting the test soil used for the desiccation stress tests in a cylindrical mold. The triaxial test apparatus employed by Oka et al. (2010) was used. It measures the lateral deformation of a specimen using four proximity transducers, symmetrically installed at heights of 20 mm and 70 mm from the bottom of the specimen. A minimum confining pressure of 20 kPa was utilized; the pressure was accurately controlled by the apparatus. Suctions of 10, 30, and 80 kPa were applied using the pressure plate method and kept constant during the shear process by allowing the pore water and pore air to drain. The range in suction corresponds to gravimetric water contents of 30.5–21.8% based on the w-SWCC, which covers the range in gravimetric water contents from the start of the test until crack initiation in the desiccation stress tests. Each specimen was sheared at a constant rate of 0.1%/min. Fig. 17 shows Poisson’s ratio when the axial strain was less than 1%. Assuming that Poisson’s ratio is constant within the range of suction, the mean value was 0.19 and the standard variation was 0.07. This indicates that approximately 70% of the specimens had a Poisson’s ratio of 0.12–0.26.

The tensile stresses induced during the desiccation stress tests were predicted using Eq. (14) and the w-SWCC shown in Fig. 6 (a), assuming that Poisson’s ratio was 0.12, 0.19, or 0.26. The computed tensile stresses are shown in Fig. 18. The figure indicates that the tensile stresses were significantly influenced by Poisson’s ratio. The measured tensile stress–gravimetric water content relationships for the 13 cases are also shown in Fig. 18. The data logging intervals

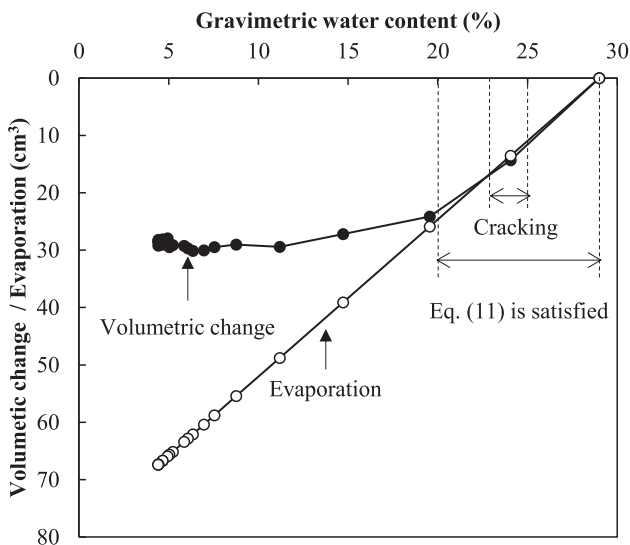


Fig. 16. Comparison between volumetric change and evaporation.

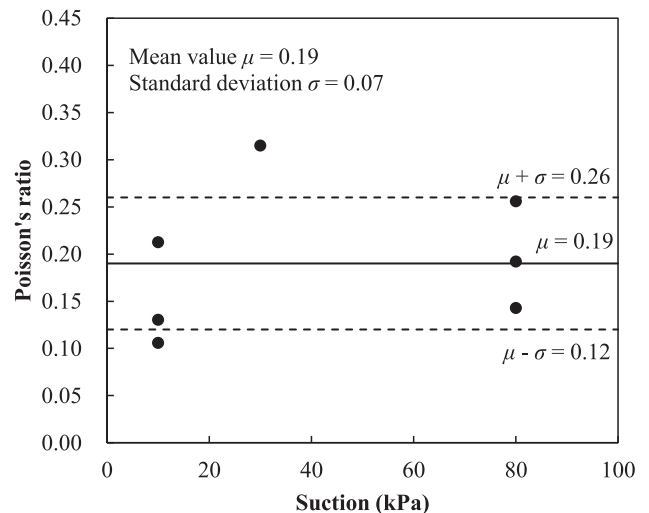


Fig. 17. Poisson’s ratio measured with drained shear tests.

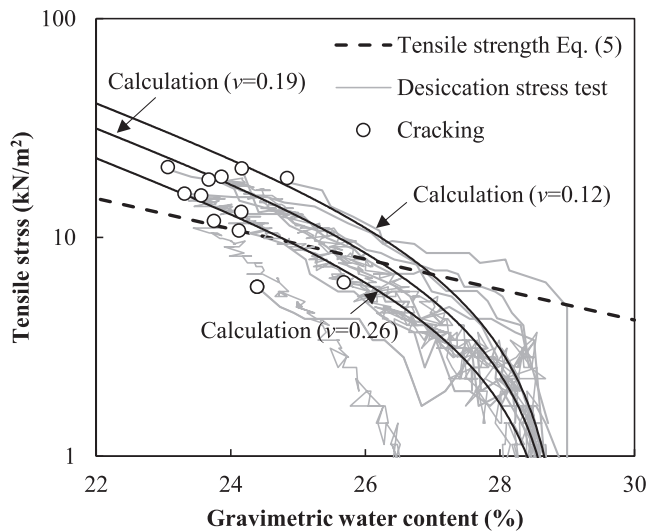


Fig. 18. Comparison between measured and computed tensile stresses.

were 10 min for nine cases and 1 min for the other four cases. The cracking points represented by circles and the tensile strength line are the same as those shown in Fig. 15. Most of the experimentally obtained curves are consistent with the curves computed with Poisson's ratios of 0.12–0.26. A comparison of the computed and measured tensile stresses shows that this model yields a reasonable tensile stress if Poisson's ratio and the SWCC are appropriately determined. Without the results of the desiccation stress tests, the tensile stress would be underestimated for two reasons. The first reason is the overestimation of Poisson's ratio, which is generally determined by referring to commonly used values that are larger than the measurements in this study because the ratio is difficult to measure. The second reason is the time lag that exists between the actual crack initiation and the visually observed crack initiation, which leads to the underestimation of the tensile stress (Section 5.1). If the water content is measured when the crack initiation is visually observed, Poisson's ratio can be determined by fitting the computed tensile stress to the tensile strength at the measured water content. However, the measured water content will be lower than the water content at the actual crack initiation. Thus, the time lag results in the overestimation of Poisson's ratio and the subsequent underestimation of the tensile stress. The desiccation stress test enables the determination of an appropriate Poisson's ratio that gives the actual tensile stress and accurately predicts the crack initiation.

6. Conclusions

This study presents the development of a desiccation stress test to measure the induced tensile stress during the drying process until crack initiation. Desiccation stress tests were performed on sandy soil with a rich fine fraction, and the results were verified by photographic observations of crack initiation and comparisons with the results of direct tension tests. The results of the desiccation stress

tests were applied to verify an existing model for crack initiation by desiccation. The results of this study are summarized as follows:

- (1) The tensile stress measured with the desiccation stress test is consistent with the photographic observation of the crack initiation. The desiccation stress test has the advantage of accurately detecting the crack initiation, as well as of measuring the tensile stress until the crack initiation because it detects the crack initiation by measuring the peak tensile stress until a crack apparently opens.
- (2) The peak tensile stress values measured by the desiccation stress tests are almost equivalent to the tensile strengths measured by the direct tension tests. This shows that the desiccation stress test yields quantitatively reliable tensile stress measurements until the crack initiation.
- (3) The results of desiccation stress tests are useful for determining the model parameters that significantly influence the development of tensile stress. It is possible to determine the appropriate parameters that yield the actual tensile stress and accurately predict the crack initiation by fitting the computed tensile stresses to the results of the desiccation stress tests.

Acknowledgments

The authors would like to thank Prof. T. Nishimura of (Ashikaga University for the useful discussions on soil mechanics in a high suction range. This work was supported by JSPS KAKENHI Grant Number 18K13827.

References

- Agency for Cultural Affairs, 2017. Report on tumuli damaged by the 2016 Kumamoto Earthquake (in Japanese).
- Agency for Cultural Affairs, Nara National Research Institute for Cultural Properties, Archeological Institute of Kashihara Nara Prefecture and Asuka Village Board of Education, 2017. Excavations report in the Takamatsuzuka tumulus, 139–148 (in Japanese).
- Fredlund, D.G., Xing, A., 1994. Equations for the soil-water characteristic curve. *Can. Geotech. J.* 31 (4), 521–532.
- Fredlund, D.G., 2017. Role of the soil-water characteristic curve in unsaturated soil mechanics. In: *Proceedings of the 19th International Conference on Soil Mechanics and Geotechnical Engineering*, 57–80.
- Fredlund, M.D., Wilson, G.W., Fredlund, D.G., 2002. Representation and estimation of the shrinkage curve. In: *Proceedings of the 3rd International Conference on Unsaturated Soils*, 145–149.
- Jommi, C., Valimberti, N., Tollenaar, R.N., Della Vecchia, G., van Paassen, L.A., 2016. Modelling desiccation cracking in a homogenous soil clay layer: comparison between different hypotheses on constitutive behavior. *E3S Web of Conferences*. EDP Sci.
- Matsushita, H., Tsuruta, H., 1999. The influences of quality of coarse aggregate on the autogenous shrinkage stress in high-fluidity concrete. *Autogenous Shrinkage of Concrete*, Taylor & Francis, London, 363–374.
- Mimura, M., Sawada, M., Yoshimura, M., Matsuura, M., 2015. A study on the compaction energy of tumulus mounds. In: *Proceedings of the 50th Annual Conference of JGS*, 23–24 (in Japanese).

- Moriguchi, T., Ogura, D., Iba, C., 2019. Study on provisional preservation in Kamao tumulus damaged by the 2016 Kumamoto Earthquake. Summaries of Technical Papers of Annual Meeting Architectural Institute of Japan, 73–74 (in Japanese).
- Nahlawi, H., Kodikara, J.K., 2006. Laboratory experiments on desiccation cracking of thin soil layers. *Geotech. Geol. Eng.* 24 (6), 1641–1664.
- Namikawa, T., Koseki, J., 2007. Evaluation of tensile strength of cement-treated sand based on several types of laboratory tests. *Soils Found.* 47 (4), 657–674.
- Ohno, Y., Nakagawa, T., 1999. Research of test method for autogenous shrinkage stress in concrete. *Autogenous shrinkage of concrete*, Taylor & Francis, London, 375–382.
- Oka, F., Kodaka, T., Suzuki, H., Kim, Y.-S., Nishimatsu, N., Kimoto, S., 2010. Experimental study on the behavior of unsaturated compacted silt under triaxial compression. *Soils and Found.* 50 (1), 27–44.
- Péron, H., Laloui, L., Hueckel, T., 2005. *Experimental evidence in desiccation cracking in sandy silt*. Taylor & Francis, Trento, Italy, pp. 475–481.
- Rodríguez, R., Sanchez, M., Ledesma, A., Lloret, A., 2007. Experimental and numerical analysis of desiccation of a mining waste. *Can. Geotech. J.* 44 (6), 644–658.
- Sawada, M., Mimura, M., Yoshimura, M., 2016. Evaluation of rainfall induced slope failure in tumulus mounds and conservation of the damaged tumuli. *JGS Special Publications* 2 (78), 2684–2689.
- Sánchez, M., Manzoli, O.L., Guimarães, L.J., 2014. Modeling 3-D desiccation soil crack networks using a mesh fragmentation technique. *Comput. Geotech.* 62, 27–39.
- Tollenaar, R.N., 2017. *Experimental investigation on the desiccation and fracturing of clay* Ph.D. thesis. Delft University of Technology.
- Towner, G.D., 1987. The mechanics of cracking of drying clay. *J. Agric. Eng. Res.* 36 (2), 115–124.
- Trabelsi, H., Jamei, M., Zenzri, H., Olivella, S., 2012. Crack patterns in clayey soils: experiments and modeling. *Int. J. Numer. Anal. Methods Geomech.* 36 (11), 1410–1433.